공학석사 학위논문

Enhancement of Light Extraction Efficiency of Photoluminescence Quantum-Dot Display by Helical Photonic Crystal

나선 광결정에 의한 광발광 양자점 디스플레이의
광추출 효율 향상에 관한 연구

2020 년 8 월

서울대학교 대학원

공과대학 전기·정보공학부

전 종 민

Enhancement of Light Extraction Efficiency of Photoluminescence Quantum-Dot Display by Helical Photonic Crystal

나선 광결정에 의한 광발광 양자점 디스플레이의
광추출 효율 향상에 관한 연구

지도교수 이 신 두

이 논문을 공학석사 학위논문으로 제출함
2020 년 8 월

서울대학교 대학원
공과대학 전기·정보공학부
전 종 민

전종민의 공학석사 학위논문을 인준함
2020 년 5 월

위 원 장	정 윤 찬	(인)
부위원장	이 신 두	(인)
위 원	곽 정 훈	(인)

Abstract

Photoluminescence quantum-dot (PL-QD) displays have attracted great interest in next-generation emissive-type displays owing to their high color purity, narrow bandwidth, and color tunable emission. Recently, QD color filters with blue organic light-emitting diode (OLED) backlights have been studied, improving color gamut and contrast ratio. However, these structures have low light extraction efficiency due to total internal reflection by the characteristics of QDs emitting light in all directions. Surface engineering and internal grating patterns, which are commonly used techniques to reduce total internal reflection, lack device uniformity and patterning accuracy required to be applied to large-area processes. In addition, light-recycling method using multilayer optical filters has also been introduced, but the cost of the fabrication process is expected to be high. Thus, it is desirable to search for a new concept of the PL-QD display for the improvement of the light extraction efficiency with better device uniformity

in large-area processing.

This thesis presents a helical photonic crystal based PL-QD display for enhancing the light extraction efficiency. The helical photonic crystal array which selectively reflects circularly polarized light within the specific wavelength range is located between the emissive QD array and the backlight, resulting in the enhancement of the light extraction efficiency by reflecting half of the downward emitted light in the QD array. From the spectroscopic analysis, it was shown that the light extraction efficiency of our device was greatly improved compared with the conventional PL-QD display. Also, it was confirmed that the color purity of the QD array was stably maintained even with the multiple photo-polymerization patterning processes. Our helical photonic crystal based PL-QD display will provide a firm basis for the next generation PL-QD displays with high light extraction efficiency and low process cost.

Keyword: Helical photonic crystal, Reactive mesogen, Photoluminescence quantum-dot display, Light extraction efficiency

Student Number: 2018-21787

Table of Contents

List of Figures

List of Tables

Chapter 1. Introduction

1.1. Photoluminescence Quantum-Dot Display

In recent years, colloidal quantum dots (QDs) have attracted great attention in photoluminescence quantum-dot (PL-QD) displays due to their high color purity, narrow bandwidth, and color tunable emission [1-5]. QDs are nano-sized semiconductor particles having PL properties. When the QDs absorb the ultra-violet (UV) photons, an electron-hole pair in the QD can be excited to the upper state, like the electron transition through the energy bandgap in the semiconductor. Then, the electron-hole pair recombination process can occur, leading to the emission of light. The wavelength of the emitted light is determined by the particle size of QDs. The QDs also have electroluminescent (EL) properties like organic light-emitting diodes (OLEDs), but EL-QD devices are currently difficult to commercialize due to

their low quantum efficiency and lifetime compared with PL-QD devices.

A widely used commercial application of QDs in display industries is quantum-dot enhancement film (QDEF) layer which is a composite of red and green QDs [6, 7]. The QDEF layer is usually located directly in front of the blue light source of the liquid crystal display (LCD). Since light from the backlight is converted to relatively pure red and green by the QDEF, the color gamut of the QDEF-LCD is much better than the conventional LCD. However, its viewing angle and contrast ratio are still insufficient compared with OLED due to the limitations of the spatial light modulation [8]. Recently, QD-OLED using blue OLED backlight and QD color filter array has attracted attention as an alternative to QDEF-LCD [9, 10]. It has the high contrast ratio like the OLED panel because each pixel can be turned off. Also, the QD color filter array performs color conversion without filtering of the light source, resulting in low light loss and high color gamut. Hence, QD-OLEDs are viewed as a potential application for the next-generation emissive-type display.

1.2. Light Extraction Techniques in Quantum-Dot Devices

In general, it is known that the light extraction efficiency, which is also called the out-coupling efficiency, is about 20 % in emissive displays based on OLED devices or QD devices [11, 12]. Light generated from the emissive layer is mostly lost due to total internal reflection and wave-guiding effect, as represented in Fig. 1.1. There have been several approaches to the enhancement of the light extraction efficiency. Recently, surface roughened substrates [13] and internal grating patterns [14] have been proposed to suppress total internal reflection. However, such systems usually lack device uniformity and have relatively low patterning accuracy, so that large area processes are not suitable for applying the above approaches. Also, optical recycling methods using long pass filter [15] or short pass filter [16] have been provided, but the fabrication process is expected to be complicated and expensive due to multiple vacuum deposition for fabricating the optical filter with inorganic multilayer films. Thus, it is desirable to find a new practicable

way for enhancing the light extraction efficiency capable of large-area processing with device uniformity.

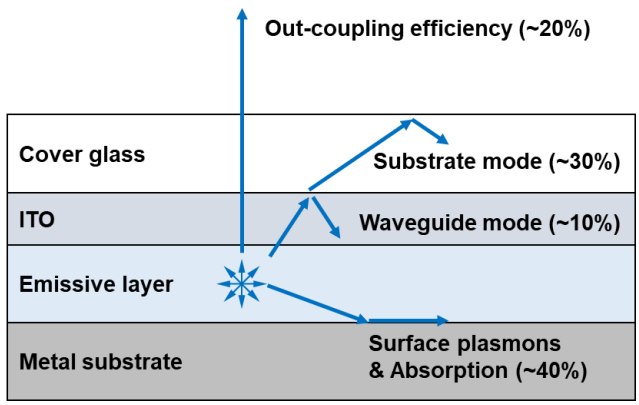

Figure 1.1. Schematic illustration of light propagation through various modes in the emissive display structure [17].

1.3. Helical Photonic Crystal Layers for High Light Extraction Efficiency

Throughout this thesis, we present a novel concept of the helical photonic crystal based PL-QD display for enhancing the light extraction

efficiency. Fig. 1.2 shows the schematic illustration of our helical photonic crystal based PL-QD display compared with the conventional PL-QD display. In general, only the upward emitted light can be extracted since QDs emit unpolarized light in all directions, as shown in Fig. 1.2(a). This means that half of the photoluminescence quantum yield of the QDs is lost.

In this work, we used the helical photonic crystal array to extract half of the downward emitted light in the emissive QD array, as shown in Fig. 1.2(b). The helical photonic crystal is a kind of twisted structure in which rod-like shaped molecules aligned in each layer rotate periodically around the vertical axis. Because of its twisted shape, the helical photonic crystal has unique optical properties that selectively reflect circularly polarized light within the specific wavelength range [18-23]. That is, half of the unpolarized emitted light is reflected from the helical photonic crystal layer and becomes reusable as a light source. The detailed operating mechanism and fabrication process of our helical photonic crystal based PL-QD display with high light extraction efficiency will be discussed in the following chapters.

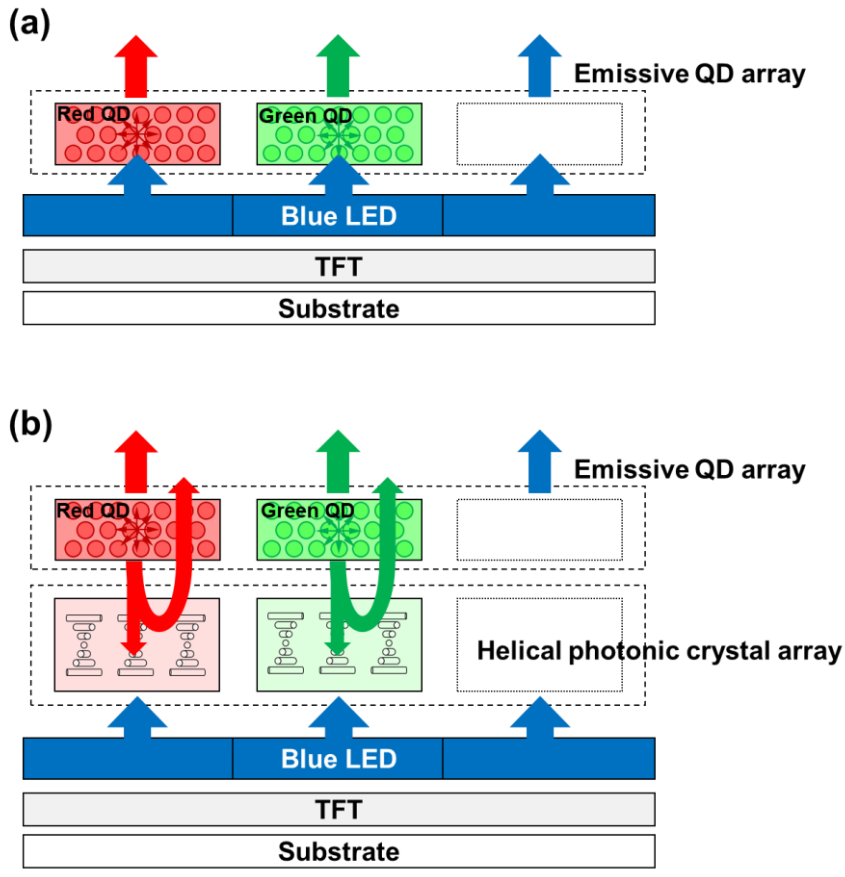

Figure 1.2. Schematic illustration of (a) the conventional PL-QD display (QD-LED) and (b) the helical photonic crystal based PL-QD display.

1.4. Outline of Thesis

This thesis consists of five chapters from Introduction to Conclusion. In Chapter 1, a general overview of the PL-QD display is provided. The brief description of several light extraction techniques in QD devices and our novel approach with helical photonic crystal layers for high light extraction efficiency are also introduced in this chapter. Chapter 2 covers the theoretical background for understanding the reactive mesogens and the selective reflection effect of the helical structure. The finite-difference time-domain method, which is one of the famous numerical analysis, is also discussed in this chapter. Chapter 3 presents the experimental procedures of this research. The fabrication process through the multiple photo-polymerization patterning and the measurement method of the fabricated device are provided as well in this chapter. In Chapter 4, the results of experiments are presented and discussed. Finally, in Chapter 5, some concluding remarks are made.

Chapter 2. Theoretical Background

2.1. Reactive Mesogens

Mesogen is a material for inducing LC properties that have both flexibility and regularity. The mesogen structure consists of rigid parts and flexible parts which characterize order and fluidity. The rigid component of the mesogen structure makes it easy to align itself in a specific direction due to its rod-like shape, and the flexible component leads to the effect of preventing crystallization to some extent.

Reactive mesogens (RMs) are chemical compounds having functional groups located on the tail of mesogen materials that can be polymerized in response to UV light or heat. The schematic diagram of the photo-polymerization process of the RMs is depicted in Fig. 2.1. As shown Fig. 2.1(a), the RMs have rod-shaped molecules as a core group and have

mono-acrylate or di-acrylate tails which causes photo-polymerization reaction when exposed to UV light. After photo-polymerization process, the RMs form liquid crystalline polymers (LCPs) as shown in Fig. 2.1(b). The LCPs, which have high thermal stability and low chemical reactivity, have a permanently fixed LC phase when aligned in a specific direction before the photo-polymerization process.

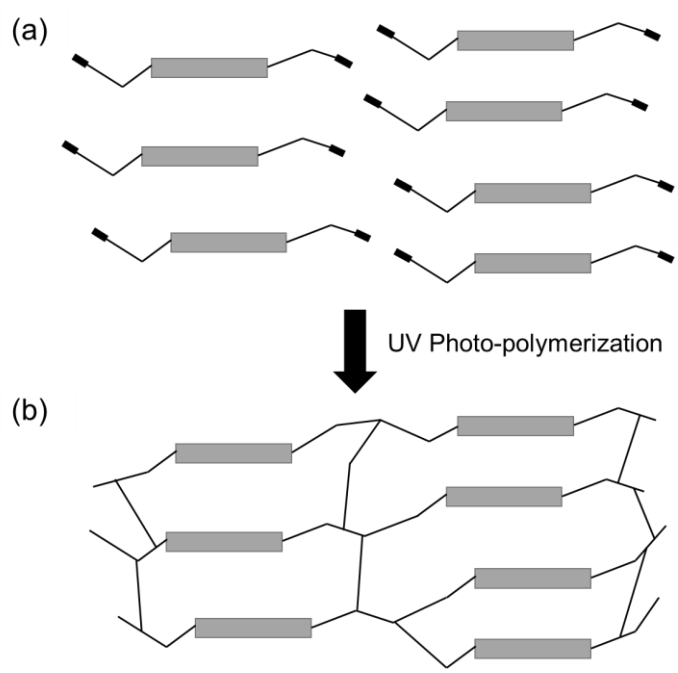

Figure 2.1. Schematic diagram of (a) the RMs and (b) the LCPs formed by the photo-polymerization of the RMs.

In addition, The RMs can be easily dissolved in organic solvents, so the LCP films are usually made by solution process such as spin-coating or dip-coating using the RM solution (RMS). Since it is possible to form stable and large-scale aligned polymer films in the simple fabrication process, the RMS has great potential in various fields where optical technology is applied, including displays.

2.2. Selective Reflection of Helical Structure

Chiral nematic phase is one of the LC phases which is made by mixing chiral dopants with LCs in nematic phase. When chiral dopants are mixed with nematic LCs, the director axis of each layer of nematic LCs is formed to rotate periodically about the vertical axis in which the twist rate of the director is uniform. As the spiral structure repeats, it becomes a helical photonic crystal, as shown in Fig. 2.2.

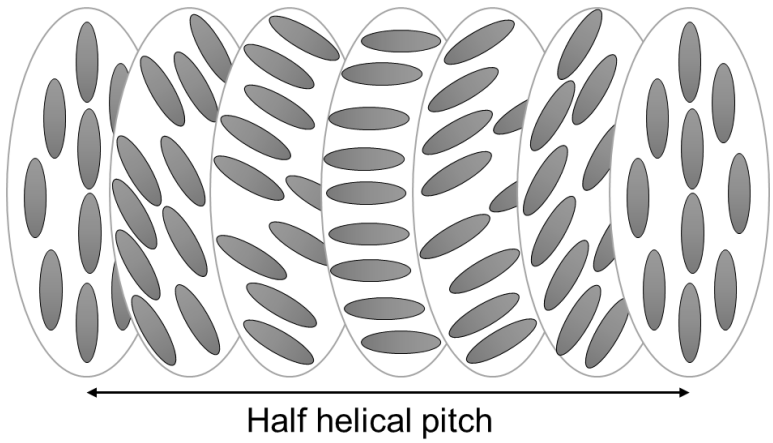

Figure 2.2. Schematic diagram of the helical photonic crystal.

The helical photonic crystal exhibits several unique optical properties, such as optical rotatory power and selective reflection of circularly polarized light. Because of the periodically rotational directors of the helical structure, circular birefringence occurs when a linearly polarized light passes through the structure. Furthermore, the helical photonic crystal reflects a circularly polarized light within a specific wavelength range, which is called selective reflection. The selective reflection effect is a result of the periodic variation of the dielectric constant along the helical axis, and the fundamental principle

is based on Bragg reflection.

When light propagates parallel to the helical axis, Bragg reflection occurs within the following wavelength range [24].

$$n_o p < \lambda < n_e p \tag{2.1}$$

$$\lambda_{peak} = \sqrt{\frac{n_e^2 + n_o^2}{2}} \cdot p \tag{2.2}$$

The wavelength range and the peak wavelength (λ_{peak}) of the reflection are determined by the helical pitch (p) and the principal refractive indices of the medium (n_o: ordinary refractive index, n_e: extraordinary refractive index). The reflected light is circularly polarized with same handedness of the helical structure. If the structure is twisted in a right-handed direction, only the right-handed polarized light within the wavelength range is strongly reflected, whereas the left-handed polarized light is transmitted. On the other hand, the left-handed polarized light is strongly reflected in the left-handed helical structure. Therefore, 50 % of the power of the unpolarized light satisfying Bragg's condition is selectively reflected and the remaining component is

transmitted through the helical structure, as depicted in Fig. 2.3.

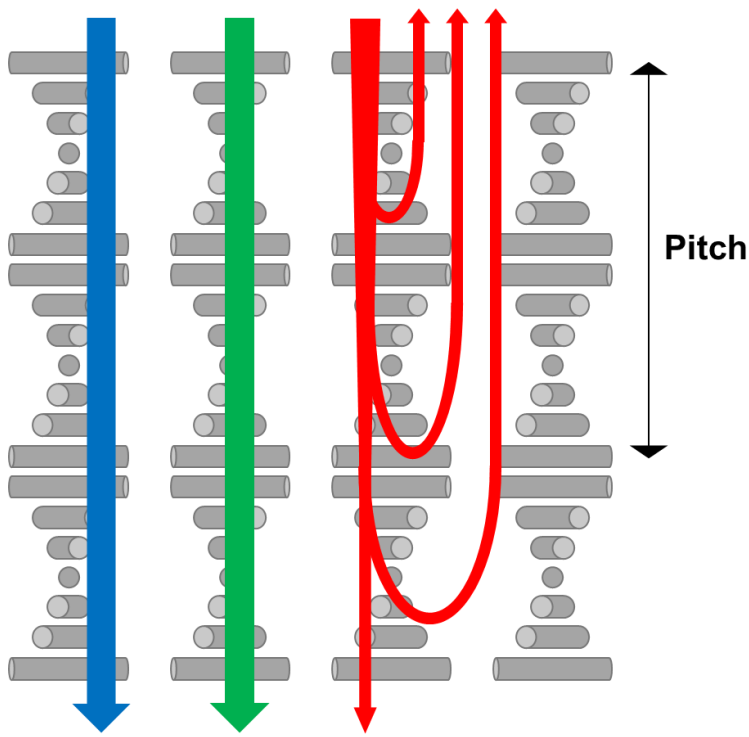

Figure 2.3. Schematic diagram of the selective reflection of the helical structure satisfying Bragg's condition in the red wavelength range.

As we can see from the Eqs. (2.1) and (2.2), the wavelength range and the peak wavelength depend on the pitch of the helical structure which is determined by the amount of chiral dopant in the LC medium. That is, as the

shorter the pitch, the more blue-shifted reflected light is obtained. Conversely, the longer the pitch, the more red-shifted reflected light is obtained. In addition, the bandwidth of the reflectance spectrum is determined by the difference of the principal refractive indices.

Chiral RMs with the chiral nematic phase are blends of the chiral dopants and RMs. Also, any pitch length of the chiral RMs can be obtained by adjusting the ratio of the chiral dopants in the solution. Since the chiral RMs are also photo-polymerizable and easily dissoluble in organic solvents, it is possible to create a stable and large-scale helical photonic crystal by solution process [25-27].

2.3. Finite-Difference Time-Domain Method

Finite-difference time-domain (FDTD) method is one of the famous numerical analysis techniques used in computational electrodynamics

proposed by K. Yee in 1966 [28]. Since it is time-domain method, a wide range of frequency responses can be calculated with a single simulation run. Also, it can be applied in any electrodynamics problems related to the Maxwell's equations.

The basic idea of the FDTD method is to apply central difference approximation to the time and spatial derivatives of the Maxwell's equations. To do this, it is necessary to define a system called Yee grid that discretizes time and space. Fig. 2.4 shows the schematic diagram of the Yee grid for the one-dimensional FDTD method. As we can see, the electric field and the magnetic field have shifted each other in the spatial domain by half of the unit length. In the same way, they have also shifted each other in the time domain by half of the unit time. This grid system that lags in half is directly connected to the central difference approximation of the Maxwell's curl equations.

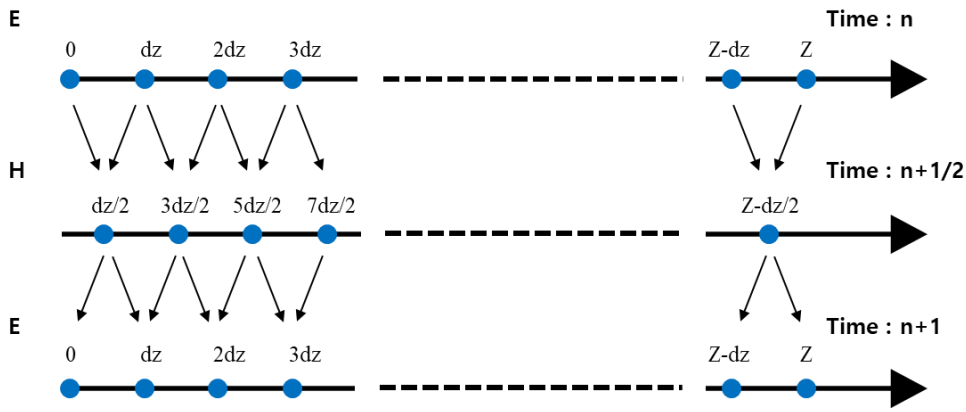

Figure 2.4. Schematic diagram of the Yee grid for the one-dimensional FDTD method.

Let us assume the light propagates through some dielectric medium in free space. The Maxwell's curl equations can be written as

$$-\mu_0 \frac{\partial H}{\partial t} = \nabla \times E \tag{2.3}$$

$$\frac{\partial D}{\partial t} = \varepsilon \frac{\partial E}{\partial t} = \nabla \times H \tag{2.4}$$

In the one-dimensional case, only the E_x and H_y components need to be considered. Then, the modified equations by applying the central difference approximation are as follows

$$-\mu_0 \frac{H_y^{n+1/2}(k+1/2) - H_y^{n-1/2}(k+1/2)}{\Delta t} = \frac{E_x^n(k+1) - E_x^n(k)}{\Delta z} \quad (2.5)$$

$$\varepsilon \frac{E_x^{n+1}(k) - E_x^n(k)}{\Delta t} = -\frac{H_y^{n+1/2}(k+1/2) - H_y^{n+1/2}(k-1/2)}{\Delta z} \quad (2.6)$$

As shown in Fig. 2.4 and Eq. (2.5), H((k+1/2)Δz) at the time step n+1/2 is derived by E((k+1)Δz) at the time n, E(kΔz) at the time n, and H((k+1/2)Δz) at time n-1/2. Also, Eq. (2.6) depicts that E(k) at the time step n+1 is obtained by E(k) at the time n, H((k+1/2)Δz) at the time n+1/2, and H((k-1/2)Δz) at the time n+1/2. Therefore, by combining these two processes, the electromagnetic field of the future time step can be calculated by the electromagnetic field of the current time step.

Each layer of the helical photonic crystal with the chiral nematic phase has the uniaxial anisotropic behavior. In order to apply FDTD method in the helical photonic crystal medium, the dielectric constant of Eq. (2.6) must be represented as a tensor. The dielectric tensor of the helical photonic crystal is simply defined as the following [29]

$$\varepsilon(z) = \varepsilon_0 \begin{pmatrix} \beta + \alpha cos\,(2qz) & \alpha sin\,(2qz) & 0 \\ \alpha sin\,(2qz) & \beta - \alpha cos\,(2qz) & 0 \\ 0 & 0 & n_o^2 \end{pmatrix} \tag{2.7}$$

$$\beta = \frac{1}{2}(n_e^2 + n_o^2) \tag{2.8}$$

$$\alpha = \frac{1}{2}(n_e^2 - n_o^2) \tag{2.9}$$

$$q = \frac{2\pi z}{p} \tag{2.10}$$

where $n_o\ and\ n_e$ are the principal refractive indices and p is the helical pitch.

Chapter 3. Experiments

3.1. Preparation of Chiral Reactive Mesogen Layers

For verifying our proposed helical photonic crystal based PL-QD display, it is necessary to obtain the optimized chiral RM layers that selectively reflect the emitted light from the QD patterns. The materials for fabricating the layers were acrylate-based chiral RM mixtures dispersed in toluene (RMS11-067, RMS11-068; Merck). The peak wavelengths of the maximum selective reflection of RMS11-067 and RMS11-068 are 520 nm and 620 nm, respectively. The RMS11-068 was used directly to fabricate the red colored chiral RM layer. For the green colored chiral RM layer with 540 nm peak wavelength, the mixture of the RMS11-067 and RMS11-068 at 8:2 weight ratio was prepared. Since these RMS are composed of the same kind of RMs with different chiral dopant concentrations, various helical pitches

can be obtained by simply mixing the above solutions.

First, glass substrates were cleaned using acetone in an ultrasonic cleaner for about 15 min and using water for about 10 min in the same way. Next, the glass substrates were fully dried with nitrogen gas. In order to control the orientation of the chiral RMS, the homogeneous alignment layer (SE-6514H; Nissan Chemical Industries) was spin-coated on the cleaned glass substrate at the rate of 3000 rpm for 30 s and post-annealed at 180 ℃ for 1 h. Then, the alignment layer was rubbed in the horizontal direction. The red colored chiral RMS with 620 nm peak wavelength and the green colored chiral RMS with 540 nm peak wavelength were independently spin-coated on the alignment layer at the rate of 3500 rpm for 30 s. These substrates were softly annealed at 55 ℃ for 1 min to remove the solvent and cooled at room temperature for 1 min. The coated layers were photo-polymerized under the UV exposure at the intensity of 20 mW/cm^2 for 1 min. After resting at room temperature for about 1 min, the chiral RM layers with selective reflection were constructed.

3.2. Fabrication of Helical Photonic Crystal Based Quantum-Dot Devices

The polymerizable groups at tails of the chiral RMs form cross-links in areas exposed to the UV light. The cross-links have chemical non-reactivity, high thermal resistance, good reliability against moisture, and insolubility in most solvents, unlike in areas without the UV exposure. Since these photo-polymerization process of the chiral RMs is similar to the photo-lithography process of the negative photoresists, the helical photonic crystal patterns can be easily obtained using the photomask.

For the patterning of the color separated QD arrays, the red and green QDs (CZO-620T, CZO-530T; ZEUS Co., Ltd.) dispersed uniformly in the homeotropic RMS (RMS16-088; Merck) at volume ratio of 1:1 were prepared, respectively. These QD hybrid patterns were constructed by the photo-polymerization process like the helical photonic crystal patterns. It was also found that the molecular ordering of photo-polymerized RMs prevented the

aggregation of the QDs, which resulted in the improved absorption of the excitation light in the QD hybrid patterns.

The detailed fabrication process of the helical photonic crystal based QD devices is shown in Fig. 3.1. First, the homogeneous alignment layer was prepared on the cleaned glass substrate at the spin-coating rate of 3000 rpm for 30 s as shown in Fig. 3.1(a). After post-annealing process of the alignment layer at 180 ℃ for 1 h followed by rubbing in the horizontal direction, the red chiral RMS were spin-coated on the substrates at 3500 rpm for 30 s, and softly annealed at 55 ℃ for 1 min as shown in Fig. 3.1(b). The red chiral RM layer was photo-polymerized with the photomask by the exposure of the UV lamp at the intensity of the 20 mW/cm^2 for 1 min, as depicted in Fig. 3.1(c). The un-polymerized RMs were removed by toluene, and fully dried at 60 ℃. After that, the red chiral RM patterns were formed as shown in Fig. 3.1(d). The same fabrication process was applied to the green chiral RMS as shown in Figs. 3.1(e) and (f).

Next, the UV ozone (UVO) treatment was performed for 10 min to

increase wettability and adherence of the QD-RM mixtures on the chiral RM layer surface. Then, the solution with red QDs dispersed in the homeotropic RMS was spin-coated on the chiral RM patterns at the rate of 2500 rpm for 30 s. The substrate was softly annealed at 55 ℃ for 1 min to remove the residual solvent. The red QD-RM mixture was photo-polymerized with the photomask under the UV lamp at the intensity of the 20 mW/cm^2 for 1 min, as depicted in Fig. 3.1(g). The un-polymerized QD-RM mixture was washed by toluene, and the substate was fully dried at 60 ℃, resulting in Fig. 3.1(h). The same fabrication process was applied to the green QD-RM mixture as shown in Fig. 3.1(i). As a result, the helical photonic crystal based QD hybrid patterns were fabricated, as shown in Fig. 3.1(j).

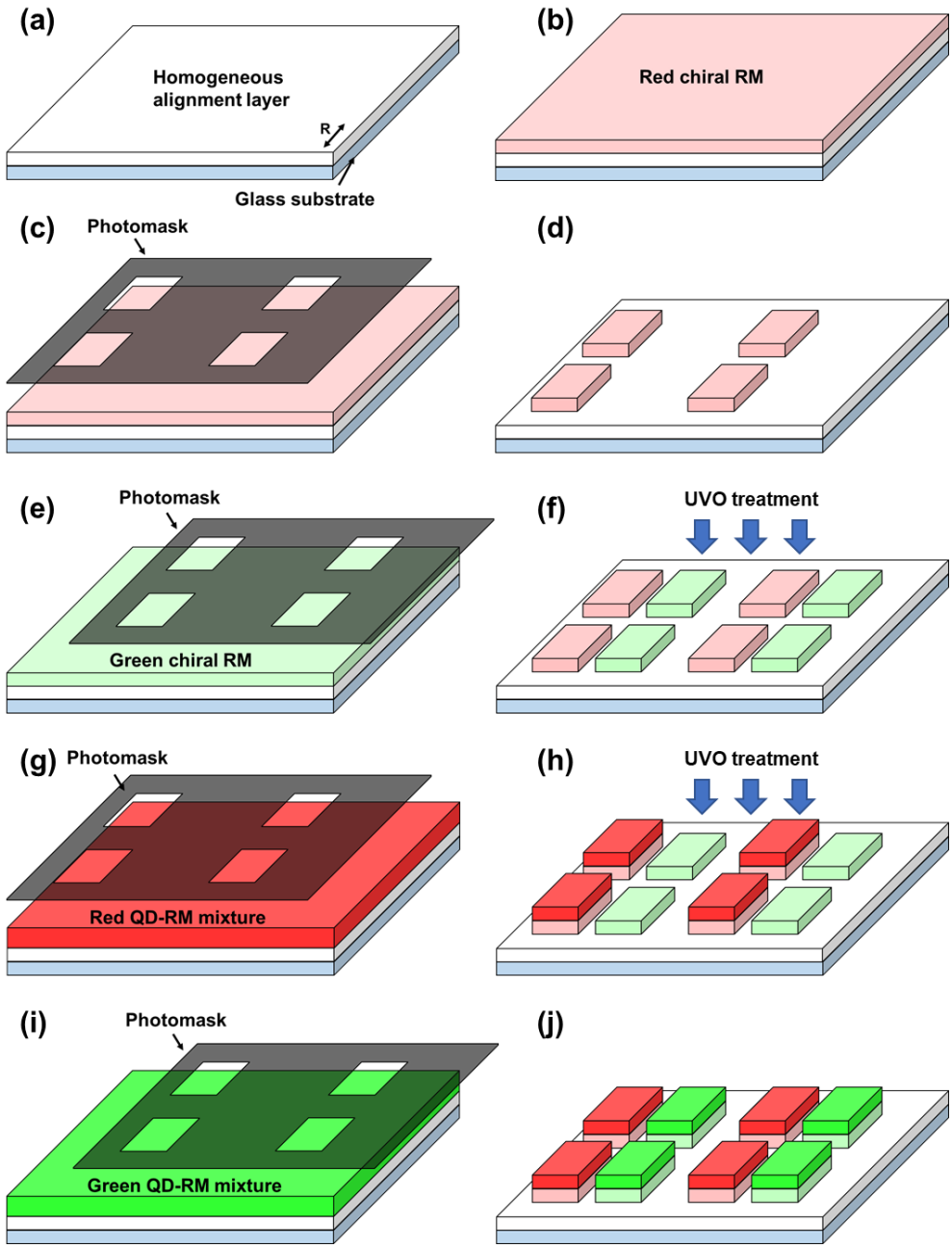

Figure 3.1. Illustration of fabrication process of the helical photonic crystal based QD hybrid patterns.

3.3. Measurements of Optical and Photoluminescence Characteristics

The red and green chiral RM film thickness were observed by the surface profiler (DektakXT; Bruker Corporation). The optical characteristics of the chiral RM layer including reflectance and transmittance were measured using the UV-VIS-NIR light source (DH-mini; Ocean Optics) and the fiber optic spectrometer (USB2000+; Ocean Optics). The UV LED light source (LLS-365; Ocean Optics) was used for emitting the helical photonic crystal based QD hybrid patterns, and the photoluminescence properties were carried out using the fiber optic spectrometer.

Chapter 4. Results and Discussion

4.1. Optimization of Helical Photonic Crystal Film Using Finite-Difference Time-Domain Method

In order to achieve the improved light extraction efficiency of the PL-QD display using selective reflection, it is important to find out the optimized thickness of the helical photonic crystal film. The FDTD simulation was performed to determine the adequate thickness that guarantees the reflectance greater than 40%. In the simulation, ordinary and extraordinary refractive indices were 1.45 and 1.59, respectively, which were the same as the values of RMS11-068. For the purpose of obtaining visible light frequency responses in one simulation, we used the broadband Gaussian pulse as the input source wave, which is described in Eq. (4.1), where the pulse duration τ is 5.8374×10^{-16} s.

$$E_{input}(t) = exp(-(t - 6\tau)^2/\tau^2) \quad (4.1)$$

Fig. 4.1 shows the FDTD simulation results of the reflectance spectra of the red, green, and blue colored chiral RM layers with different thicknesses. The peak wavelengths and helical pitches for each chiral RM layer are shown in Table 4.1. As shown in Fig. 4.1(a), which describes the reflectance spectra of the red chiral RM layer with the peak wavelength of 620 nm, the maximum reflectance rises from about 4.5 % to 40 % when the film thickness increases from 1 to 5 times the red helical pitch. Also, the full width at half maximum (FWHM) of the reflectance spectra decreases, so that the chiral RM layer reflects selectively and precisely within the suggested wavelength range. As shown in Fig. 4.1(b) and (c), It has been obtained the same results in the green and blue chiral RM layer with the peak wavelength of 540 nm and 460nm, respectively.

The above result means that the maximum selective reflectance for the enhancement of the light extraction efficiency is proportional to the film thickness. In other words, the chiral RM layer having the thickness of at least

5 times its helical pitch is required to obtain high light extraction efficiency over 30 %. Under these conditions, the optimized thicknesses of the red, green, and blue helical photonic crystal layers are 2.04 μm, 1.78 μm, and 1.51 μm, respectively.

	Red chiral	Green chiral	Blue chiral
λ_{peak}	620 nm	540 nm	460 nm
pitch (P_x x = R, G, B)	408 nm	355 nm	302 nm

Table 4.1. The helical pitches corresponding to the peak wavelengths for each chiral RM layer.

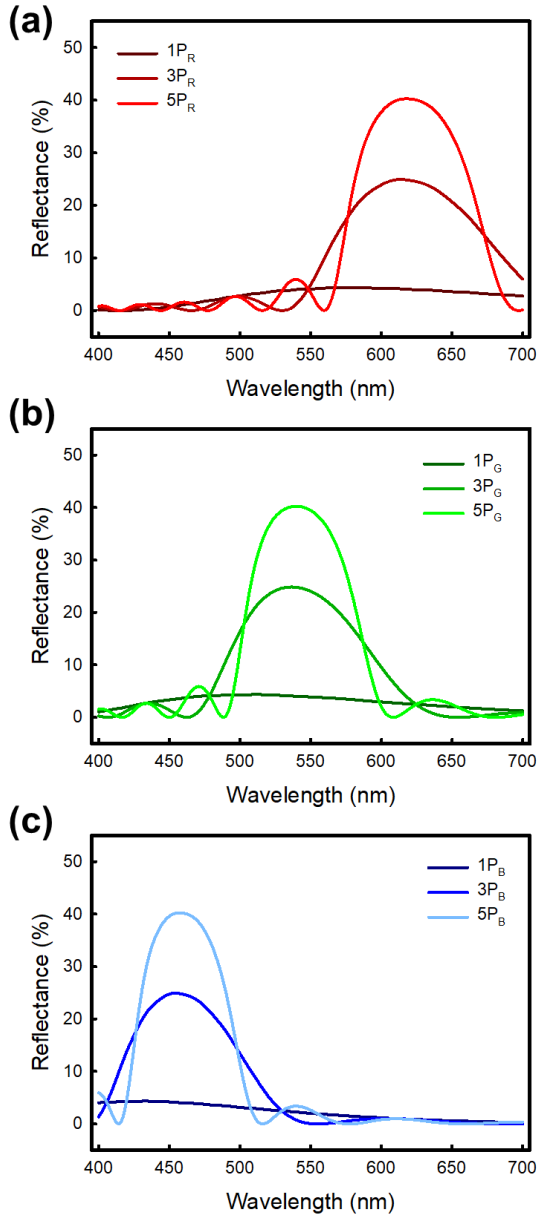

Figure 4.1. FDTD simulation results of the reflectance spectra of (a) the red chiral RM layer, (b) the green chiral RM layer, and (c) the blue chiral RM layer with different thicknesses.

4.2. Reflectance and Transmittance of Chiral Reactive Mesogen Layers

Fig. 4.2 shows the comparison of the experimental results with the simulation of the red chiral RM layer with the peak wavelength of 620 nm and the green chiral RM layer with the peak wavelength of 540 nm. These optical characteristics of the chiral RM layers were measured using the fiber optic spectrometer. It was found that the thickness of the red chiral RM layer was 2.04 μm, which corresponds to 5 times the red helical pitch, by performing the measurement with the surface profiler. In the same way, the thickness of the green chiral RM layer was measured to be 2.30 μm corresponding to 6.5 times the green helical pitch.

As a result of comparison with the simulation performed according to the above pitch length and thickness, the experimental results are consistent with the reflectance spectra expected in the simulation within the wavelength range satisfying the Bragg condition. The maximum reflectance

measurements of the red chiral RM layer and the green chiral RM layer are found to be about 39.0% and 44.7%, respectively, as shown in Fig. 4.2. In addition, the sum of reflectance and transmittance is almost 100 % in the entire visible wavelength range, which means there is no energy loss in the chiral layer. These chiral layers have 10 % reflectance outside their selective reflection wavelength range unlike the theoretical results. However, the above error does not actually affect the light extraction efficiency, due to the wider FWHM of the chiral layers compared with that of the QDs.

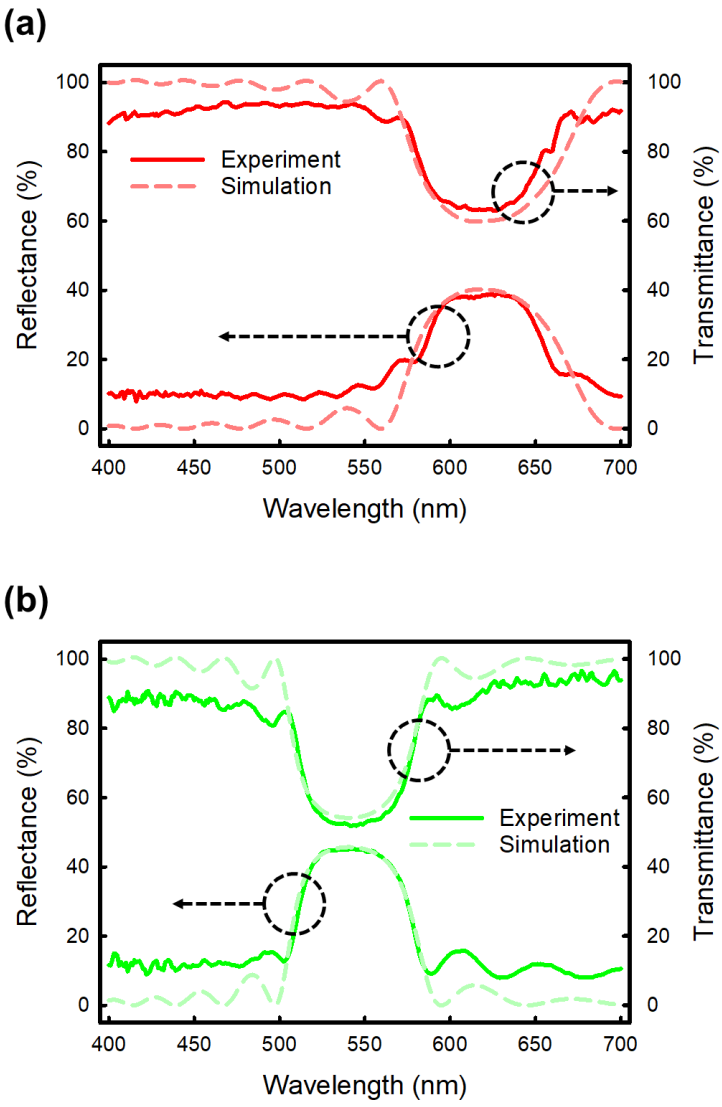

Figure 4.2. Simulated (dashed line) and measured (solid line) reflectance and transmittance spectra of (a) the red chiral RM layer and (b) the green chiral RM layer. The upper part of each graph is the transmittance and the lower part is the reflectance.

4.3. Photoluminescence Characteristics of Helical Photonic Crystal Based Quantum-Dot Devices

Our helical photonic crystal based QD films and the conventional QD films were fabricated to demonstrate the enhancement of the light extraction efficiency. The emission characteristics of these devices were measured using the fiber optic spectrometer under the UV excitation light of 365 nm wavelength.

Fig. 4.3 shows the comparison of the emission spectra of QD films with or without the helical photonic crystal layers. As shown in Fig. 4.3(a), the light extraction efficiency of the red QD film with the red chiral RM layer is improved by 40 % at the peak wavelength and 31 % on average compared with the conventional red QD film. Also, as shown in Fig. 4.3(b), the light extraction efficiency of the green QD film with the green chiral RM layer is improved by 44 % at the peak wavelength and 40 % on average. The dashed line in each graph represents the estimate obtained by adding the QD

spectrum without the chiral RM layer to the selective reflection ratio of Fig. 4.2. Since the measured emission spectra of our helical photonic crystal based QD devices coincide with their estimated spectra, it is clearly proved that the improvement of the light extraction efficiency was caused by the selective reflection effect.

Fig. 4.4 shows the measured emission spectra of our helical photonic crystal based red QD device compared with the conventional device by changing the power of the UV excitation light. As the backlight power increases, the irradiance increases while the light extraction efficiency improved by 40 % at the peak wavelength is maintained every moment. In other words, it is observed that the improved light extraction efficiency is maintained stably regardless of the input power.

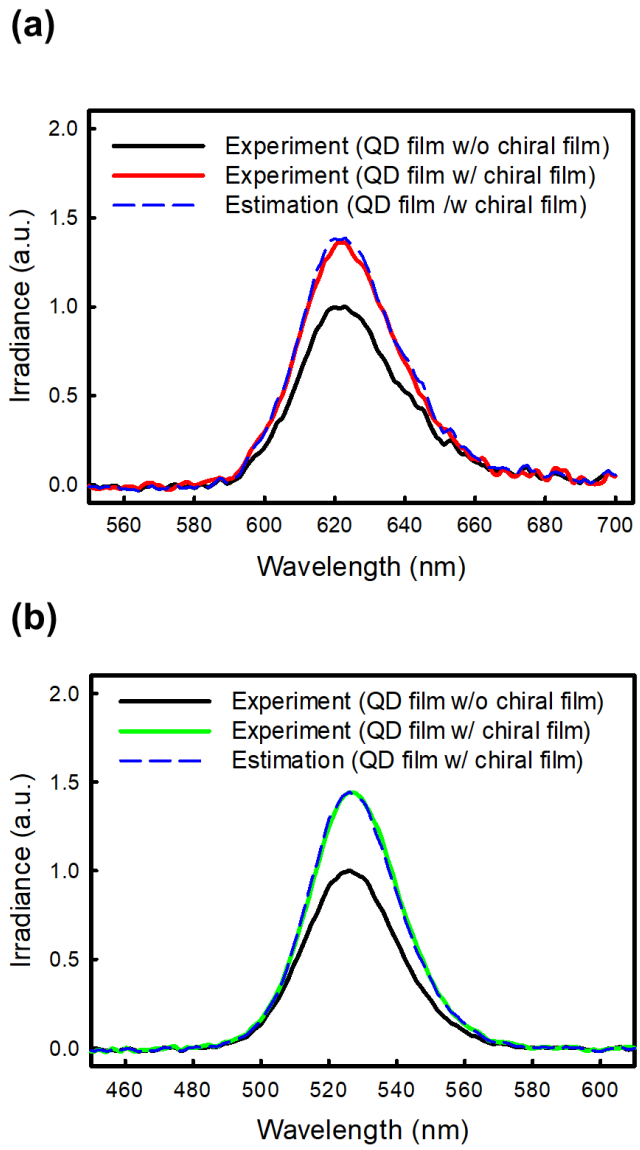

Figure 4.3. Estimated (dashed line) and measured (colored solid line) emission properties of our helical photonic crystal based (a) red QD device and (b) green QD device under the UV excitation light compared with the emission spectrum of the conventional QD devices (black solid line).

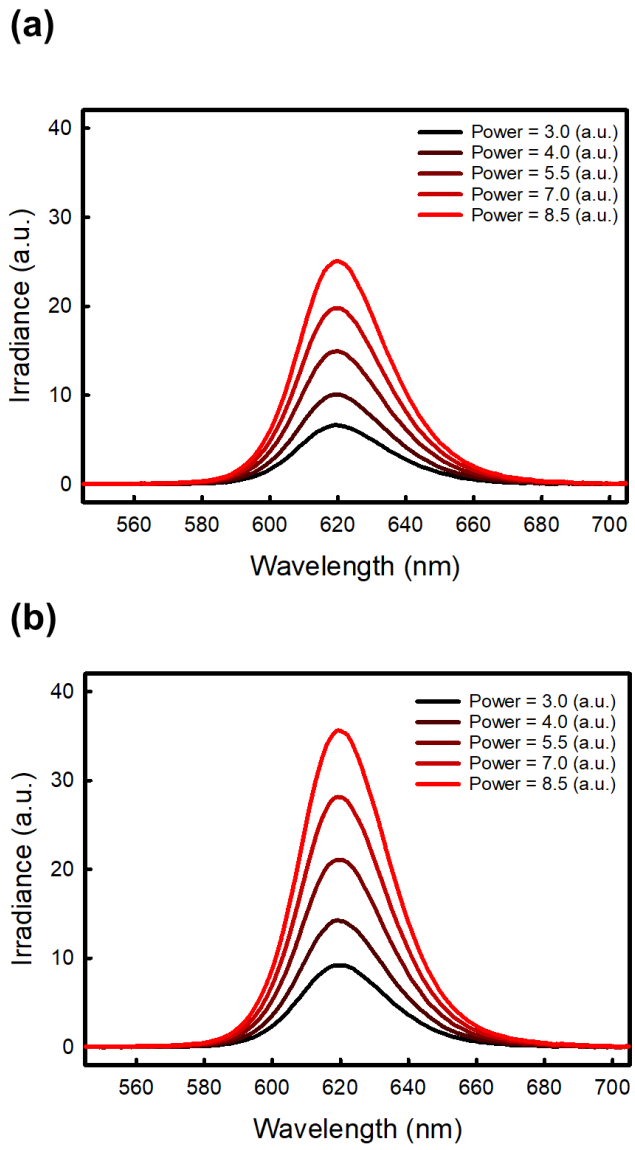

Figure 4.4. Measured emission characteristics of (a) the conventional red QD device and (b) our helical photonic crystal based red QD device by changing the backlight power.

4.4. Microscopic Images of Helical Photonic Crystal Based Photoluminescence Quantum-Dot Display

For the purpose of showing that our patterning process is practicable, the color pixel array of our helical photonic crystal based QD display was fabricated. Fig. 4.5 shows the emission characteristics with the microscopic images of the helical photonic crystal based monochromatic QD patterns compared with un-patterned films. The emission characteristics of the red QD pattern with the red chiral RM pattern and the green QD pattern with the green chiral RM pattern are maintained within the range where the FWHM increased by about 1.5% and 0.9%, respectively. This means that the color purity of the QDs remains stable during our pattering process.

Fig. 4.6 shows the microscopic image and emission spectrum of color pixel array of our proposed helical photonic crystal based QD display. As shown in Fig. 4.6(a), it is observed that the color pixel array is formed uniformly without any defects. Also, it has been shown that the QD hybrid

patterns are coated directly above the underlying chiral RM patterns without any alignment issues. In addition, the emission spectrum remains constant without significant changes even with the multiple photo-polymerization patterning processes for fabricating the emissive patterns on the reflective patterns, as shown in Fig. 4.6(b).

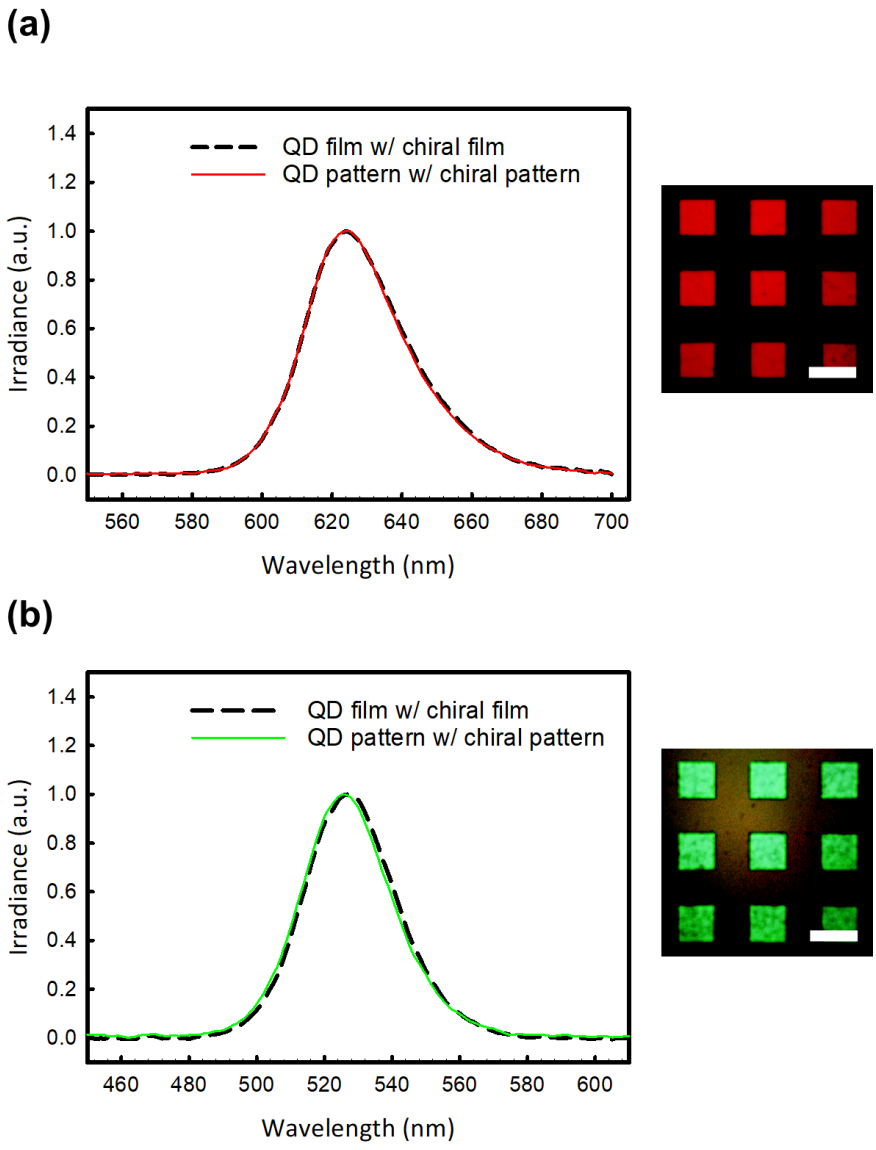

Figure 4.5. Microscopic images and emission characteristics (solid line) of our helical photonic crystal based (a) red QD pattern and (b) green QD pattern, compared with the un-patterned QD films (dashed line). Scale bars represent 300 μm.

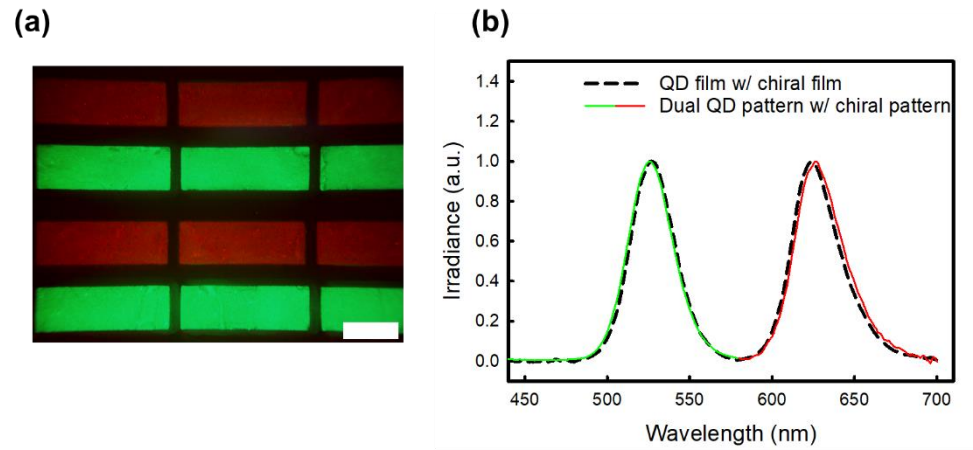

Figure 4.6. Microscopic image and emission spectrum (solid line) of color pixel array of our helical photonic crystal based QD display compared with the unpatterned film (dashed line). Scale bars in the inset are 300 μm.

Chapter 5. Conclusion

In this thesis, a novel concept of a PL-QD display with enhanced light extraction efficiency by using helical photonic crystal was proposed. To improve the light extraction efficiency of the device, the helical photonic crystal layers with the selective reflection characteristics within the wavelength range satisfying the Bragg condition were applied as reflectors under the emissive QD layers. It has been shown that our device has more than 40% improvement in the light extraction efficiency at the peak wavelength compared with the conventional device. In addition, it has been observed that the improved light extraction efficiency remains constant regardless of the backlight intensity. For the fabrication of our device, the multiple photo-polymerization patterning processes were performed without any defects and alignment issues. It has also been demonstrated that the emission spectra of QD hybrid patterns are stably maintained during the fabrication processes. Our helical photonic crystal based PL-QD display is

expected to provide a practicable solution for the fabrication of next generation PL-QD displays with high light extraction efficiency.

Bibliography

[1] Y. Shirasaki, G. J. Supran, M. G. Bawendi, and V. Bulović, “Emergence of colloidal quantum-dot light-emitting technologies,” Nature Photonics, vol. 7, no. 1, pp. 13–23 (2012).

[2] R. Zhu, Z. Luo, H. Chen, Y. Dong, and S.-T. Wu, “Realizing Rec 2020 color gamut with quantum dot displays,” Optics Express, vol. 23, no. 18, p. 23680 (2015).

[3] Y. Altintas, S. Genc, M. Y. Talpur, and E. Mutlugun, “CdSe/ZnS quantum dot films for high performance flexible lighting and display applications,” Nanotechnology, vol. 27, no. 29, p. 295604 (2016).

[4] P. Ramasamy, N. Kim, Y.-S. Kang, O. Ramirez, and J.-S. Lee, “Tunable, Bright, and Narrow-Band Luminescence from Colloidal Indium Phosphide Quantum Dots,” Chemistry of Materials, vol. 29, no. 16, pp. 6893–6899 (2017).

[5] S. Ghimire, A. Sivadas, K. Yuyama, Y. Takano, R. Francis, and V. Biju, “Quantum dot–polymer conjugates for stable luminescent displays,” Nanoscale, vol. 10, no. 28, pp. 13368–13374 (2018).

[6] Z. Luo, Y. Chen, and S.-T. Wu, “Wide color gamut LCD with a quantum dot backlight,” Optics Express, vol. 21, no. 22, p. 26269 (2013).

[7] H. Chen, J. He, and S.-T. Wu, “Recent Advances on Quantum-Dot-Enhanced Liquid-Crystal Displays,” IEEE Journal of Selected Topics in Quantum Electronics, vol. 23, no. 5, pp. 1–11 (2017).

[8] Z. Luo, D. Xu, and S.-T. Wu, “Emerging Quantum-Dots-Enhanced LCDs,”

Journal of Display Technology, vol. 10, no. 7, pp. 526–539 (2014).

[9] Y. H. Kim, S. Koh, H. Lee, S.-M. Kang, D. C. Lee, and B.-S. Bae, “Photo-Patternable Quantum Dots/Siloxane Composite with Long-Term Stability for Quantum Dot Color Filters,” ACS Applied Materials & Interfaces, vol. 12, no. 3, pp. 3961–3968 (2019).

[10] Z. Hu, Y. Yin, M. U. Ali, W. Peng, S. Zhang, D. Li, T. Zou, Y. Li, S. Jiao, S. Chen, C.-Y. Lee, H. Meng, and H. Zhou, “Inkjet printed uniform quantum dots as color conversion layers for full-color OLED displays,” Nanoscale, vol. 12, no. 3, pp. 2103–2110 (2020).

[11] K. Saxena, V. K. Jain, and D. S. Mehta, “A review on the light extraction techniques in organic electroluminescent devices,” Optical Materials, vol. 32, no. 1, pp. 221–233 (2009).

[12] R. Meerheim, M. Furno, S. Hofmann, B. Lüssem, and K. Leo, “Quantification of energy loss mechanisms in organic light-emitting diodes,” Applied Physics Letters, vol. 97, no. 25, p. 253305 (2010).

[13] Q. Zhang, X. Gu, Z. Chen, J. Jiang, Z. Zhang, J. Wei, F. Li, X. Jin, Y. Song, and Q. Li, “Enhancing extraction efficiency of quantum dot light-emitting diodes by surface engineering,” Optics Express, vol. 25, no. 15, p. 17683 (2017).

[14] S. Wang, X. Dou, L. Chen, Y. Fang, A. Wang, H. Shen, and Z. Du, “Enhanced light out-coupling efficiency of quantum dot light emitting diodes by nanoimprint lithography,” Nanoscale, vol. 10, no. 24, pp. 11651–11656 (2018).

[15] H.-J. Kim, M.-H. Shin, and Y.-J. Kim, “Optical efficiency enhancement in white organic light-emitting diode display with high color gamut

using patterned quantum dot film and long pass filter," Japanese Journal of Applied Physics, vol. 55, no. 8S3, p. 08RF01 (2016).

[16] H.-J. Kim, M.-H. Shin, J.-Y. Lee, J.-H. Kim, and Y.-J. Kim, "Realization of 95% of the Rec 2020 color gamut in a highly efficient LCD using a patterned quantum dot film," Optics Express, vol. 25, no. 10, p. 10724 (2017).

[17] S. Ashok Kumar, J. S. Shankar, B. K Periyasamy, and S. K. Nayak, "Device engineering aspects of Organic Light-Emitting Diodes (OLEDs)," Polymer-Plastics Technology and Materials, vol. 58, no. 15, pp. 1597–1624 (2019).

[18] E. Plum and N. I. Zheludev, "Chiral mirrors," Applied Physics Letters, vol. 106, no. 22, p. 221901 (2015).

[19] V. P. Tondiglia, M. Rumi, I. U. Idehenre, K. M. Lee, J. F. Binzer, P. P. Banerjee, D. R. Evans, M. E. McConney, T. J. Bunning, and T. J. White, "Electrical Control of Unpolarized Reflectivity in Polymer-Stabilized Cholesteric Liquid Crystals at Oblique Incidence," Advanced Optical Materials, vol. 6, no. 22, p. 1800957 (2018).

[20] Q. Hong, T. X. Wu, and S.-T. Wu, "Optical wave propagation in a cholesteric liquid crystal using the finite element method," Liquid Crystals, vol. 30, no. 3, pp. 367–375 (2003).

[21] R. J. Hernández, A. Mazzulla, A. Pane, K. Volke-Sepúlveda, and G. Cipparrone, "Attractive-repulsive dynamics on light-responsive chiral microparticles induced by polarized tweezers," Lab Chip, vol. 13, no. 3, pp. 459–467 (2013).

[22] M. A. Christou, N. C. Papanicolaou, and A. C. Polycarpou, "Modeling

the reflection from cholesteric liquid crystals using modal analysis and mode matching," Physical Review E, vol. 85, 031702 (2012).

[23] K.-S. Bae, U. Cha, Y.-K. Moon, J. W. Heo, Y.-J. Lee, J.-H. Kim, and C.-J. Yu, "Reflective three-dimensional displays using the cholesteric liquid crystal with an inner patterned retarder," Optics Express, vol. 20, no. 7, p. 6927 (2012).

[24] P. Yeh and C. Gu, Optics of Liquid Crystal Displays (Wiley Interscience, New York, 1999)

[25] S.-U. Kim, S.-H. Lee, I.-H. Lee, B.-Y. Lee, J.-H. Na, and S.-D. Lee, "Generation of intensity-tunable structural color from helical photonic crystals for full color reflective-type display," Optics Express, vol. 26, no. 10, p. 13561 (2018).

[26] S. H. Lee, S.-H. Lee, S.-U. Kim, S. Kang, and S.-D. Lee, "Concept of chiral image storage and selection based on liquid crystals by circular polarization," Optics Express, vol. 27, no. 8, p. 11661 (2019).

[27] Y. Inoue and H. Moritake, "Dynamic control of colorful reflection toward practical cholesteric liquid crystal displays," Optics Express, vol. 24, no. 20, p. 23027 (2016).

[28] Kane Yee, "Numerical solution of initial boundary value problems involving maxwell's equations in isotropic media," IEEE Transactions on Antennas and Propagation, vol. 14, no. 3, pp. 302–307 (1966).

[29] C.-L. Ting, T.-H. Lin, C.-C. Liao, and A. Y. Fuh, "Optical simulation of cholesteric liquid crystal displays using the finite-difference time-domain method," Optics Express, vol. 14, no. 12, p. 5594 (2006).

초록

광발광 양자점 디스플레이는 높은 색순도, 좁은 선폭, 색상 가변성으로 인해 차세대 발광형 디스플레이로 주목을 받고 있다. 최근 청색 발광 다이오드를 백라이트로 하고 양자점 컬러필터 어레이를 사용하여 색순도뿐 아니라 명암비도 개선시키는 연구가 진행되어 왔다. 그러나 양자점의 사방으로 발광하는 특성에 의한 내부 전반사 효과 때문에 광 추출 효율이 낮은 문제가 있었다. 이러한 문제점을 극복하기 위해, 기판 표면을 거칠게 하거나 기판 내부에 격자 패턴을 만들어 내부전반사 효과를 줄이는 연구가 진행되어왔으나, 소자 균일성 및 패턴 정확성이 낮아 대면적 공정에 적용하기 어려운 문제를 지닌다. 또한 다층 광학 필터를 추가한 광 재사용 방식이 제안되었으나 공정 단가가 높은 단점이 있다. 따라서 소자 균일성을 유지하면서 광 추출 효율이 뛰어난

새로운 방식의 광발광 양자점 디스플레이 구조가 필수적이다.

본 연구에서는 나선 광결정을 이용하여 향상된 광 추출 효율을 갖는 광발광 양자점 디스플레이를 제안한다. 구체적으로, 특정 파장대의 원형 편광 빛을 선택적으로 반사하는 나선 광결정 패턴을 양자점 발광층 하부에 생성하여, 그 효과로 양자점으로부터 발광 된 하부로 향하는 빛 중 약 절반을 상부로 향하도록 반사하여 광 추출 효율을 향상시켰다. 발광 스펙트럼 분석 결과로부터 기존 광발광 양자점 디스플레이에 비해 광 효율이 크게 향상된 것을 보였다. 또한 다중 광경화 패터닝 공정을 수행하여도 양자점의 색 순도가 안정적으로 유지됨을 확인하였다. 우리의 나선 광결정 기반 광발광 양자점 디스플레이는 저비용의 용액공정 및 높은 광 추출 효율을 갖는 장점을 통해 차세대 발광형 디스플레이의 실용적인 해법을 제공할 수 있을 것으로 기대된다.

주요어: 나선 광결정, 반응성 메조겐, 광발광 양자점 디스플레이, 광 추출 효율

학번: 2018-21787